Bioinspired biomaterials for regenerative medicine

INTRODUCTION

Over the past few years, researchers have explored regenerative medicine using a combination of biomaterials and bioactive molecules to solve problems associated with age-related and trauma related bone disease. Traditional therapeutic approaches have a number of disadvantages including long hospitalization, highly invasive procedures, anesthesia, blood transfusions, and prolonged postoperative rehabilitation. Minimally invasive orthopedic surgery, also known as "keyhole" surgery, in combination with smart biomaterials, can be adopted in both orthopedics and dentistry to reduce the risk of complications [1].

Progress in tissue engineering, innovative and smart biomaterials and new endoscopic techniques has led to great advances in. The growing need for minimally invasive approaches has led to increased focus on the synthesis and development of smart injectable biomaterials. The present research focusses on the development of an innovative protein, Mucin as an injectable hydrogel for regenerating lost or damaged bone [2]. Mucins are large glycoproteins that coat the surfaces of many cell types and can be secreted to form mucus gels that assume important physiological roles. The increasing understanding of the structure and function of mucin molecules and their multi-functionalities has developed interest in investigating the use of mucins as building blocks for innovative functional biomaterials [3]. Some of the established properties of Mucin from which Mucin based biomaterials can benefit are excellent barrier properties, hydration and lubrication properties, unique chemical diversity, and bioactivities of mucins. Our study involves developing Mucin based scaffolds to understand the underlying mechanism of *in-vitro* mineralization so as to develop a material that can be used as an effective bone graft substitute. The developed formulation of the scaffold contained collagen and Mucin in a template of polyethylene glycol. In order to understand the molecular and residual interactions between the two involved proteins namely collagen and mucin, *in-silco* modelling and docking studies were performed as experimentally determined structures for both of these proteins are not determined. After the analysis of the docked complexes both the proteins showed a significant affinity with each other in the Insilco docking environment. The residue level interactions showed a proper inter molecular hydrogen bonded contacts between charged residues of Arginine, Glutamates of Mucin and Prolines and hydroxy prolines of Collagen. Apart from them a plenty of pi-pi and van der Waals interactions between the hydrophobic residues like Tyrosine and Phenylalanine of Mucin and Glycine and hydroxy prolines (Fig 2). These interactions are suggesting a possible strong affinity between the collagen and mucin in both *in vitro* and *in vivo* environments. Furthermore, a successfully developed Mucin scaffold shows promising cell viability (Fig 11-13) and mineralization till 28 days as observed by the live/dead assay. Positive results are indicated irrespective of the different ratios of collagen and Mucin used in fabricating the scaffold.

I. OBJECTIVES

1. Characterizing the protein, Mucin in terms of properties required for processing as a biomaterial.
2. Exploring the interaction and functionality of Mucin in the bone microenvironment using in-silico approach.
3. Employing different chemistries for developing polymeric architecture for promoting regeneration.
4. Exploring different routes for mineralization of the polymeric scaffolds.
5. In-vivo analysis of the scaffolds.

II. MATERIALS

Collagen rat tail (cat. no. C7661) and Mucin type-1S (cat. no. M3895) of the submaxillary gland from Bovine. Polyethylene glycol dimethacrylate (PEGDMA) of molecular weight (average Mn 550) (cat. no. 409510) and PEGDA of average Mn 575 (cat. no. 437441) including Irgacure 2959 was purchased from Sigma-Aldrich. Bovine intestinal ALP (Alkaline phosphatase)(specific activity: ≥ 10 DEA U/mg; cat. no. P7640) and calcium glycerol phosphate (cat. no. 50043) were obtained from Sigma-Aldrich. 1-(3-Dimethylaminopropyl)-3-Ethyl Carbodiimide Hydrochloride (EDC)(cat. no. 49235) and N-Hydroxysuccinimide (NHS) (cat. no. 47913) was purchased from SRL. Mucin type-1S (cat. no. M3895) of the submaxillary gland from Bovine and Poly(N-isopropylacrylamide) PNIPAM (Cat no- 724459-5g) was purchased from Sigma-Aldrich. 1-(3-Dimethylaminopropyl)-3-Ethyl Carbodiimide Hydrochloride (EDC)(cat. no. 49235) and N-Hydroxysuccinimide (NHS) (cat. no. 47913) was purchased from SRL. MES buffer solution was purchased from Himedia. Chitosan medium molecular weight (cat no. 448877) and ammonium persulfate (APS) (cat no. A3678) was purchased from Sigma-Aldrich. 2-Hydroxyethyl methacrylate (HEMA) (cat no. 477028), nanoclay or montmorillonite, hydrophilic bentonite (cat no. 682659) purchased from sigma and TEMED (cat no. 52145) were purchased from SRL.

III. METHODOLOGY

Objective 1:

Characterization of commercially available Mucin type 1S

SDS PAGE Analysis

Mucin type-1S purity was evaluated with sodium dodecyl sulfate-polyacrylamide gel electrophoresis (SDS-PAGE) using 8% polyacrylamide gel taking mucin in 1xPBS at the concentration of 50 mg/ml.

Then we diluted the mucin protein for SDS-PAGE gel run at the concentration of 30 µg and loaded 30 µl of mucin along with another protein, as experimental control, collagen, 30 µg of concentration with high molecular weight protein ladder. Molecular mass markers were purchased from (Thermo fisher scientific, # Cat No. LC 5688) and the gel was stained with Coomassie blue R-250 using the manufacture's protocol.

MALDI-TOF TOF

The procedure involved here is cutting protein bands or spots from 2D PAGE gels, destaining the gel pieces, reducing and alkylating the protein, digesting with trypsin, analysing using MALDI-TOF TOF mass spectrometry (Sciex 5800) to determine the mass of the tryptic peptides and database searching with the PMF data to identify the protein [33].

Circular Dichroism (CD)

CD spectra were obtained using a Jasco 1500 spectrometer. Mucin protein was prepared 2 mg/ml in 1XPBS with pH 7.4 and 1 ml of protein was used for overnight dialysis with 3 times media change. The final concentration that was used for CD spectra analysis after dialysis was 0.1 mg/mL. Samples (400 µL) were loaded into optically matched quartz cuvettes (0.1 cm path length). All ellipticity measurements were performed using the same cuvette for baselines and samples from 190-260nm wavelength. Ellipticity measurements were corrected for buffer baseline, and when possible, ellipticity was converted to mean residue ellipticity (MRE) and molecular weights were used from the NCBI database [34]. Measurement of wavelength regions 200-280 nm was done.

Objective-2

Insilco approach to check multifunctional nature of mucin protein in bone tissue engineering

In-ssilico-approach for pathway analysis

String dB tool is being used in order to know the interaction between the bone genes along with Mucin and the interaction analysis was followed by gene ontology pathway analysis in which the m-RNA linked with Mucin gene was evaluated first then mirwalk tool was used to know relevant biological processes.

In-silco modelling and molecular docking

Mucin and Collagen sequences were retrieved from Uniprot database. As these proteins do not have proper homology with the structural proteins, we have performed ab-initio modelling using Robetta Server. The Best structural models for both collagen and mucin were selected based on the validation from the SAVES server which included the tools like Procheck , Errat, verify3D etc. and ProsaWeb. Then the validated structural models were further used for protein-protein docking calculations. Protein-Protein docking was performed using HADDOCK software. Before performing the protein-protein

docking, active and passive residues were identified for both the proteins using Metapocket 2.0 server. This server uses multiple algorithms for identification of binding cavities and sites for possible ligand or binding partner interactions. After identification of the consensus binding sites, this information was used as input for initiating the protein-protein docking using HADDOCK. During the docking calculations, the final refinement was performed in water conditions. After Successful protein-protein docking calculations, the best-docked conformation between mucin and collagen was identified based on the energetics and binding conformation. Binding poses were visualized and analyzed using open-source Pymol. The Atomistic and residue level interactions were analyzed using the Ligplot+. The Best docked Mucin and Collagen structural complex was further used for the molecular dynamic simulations (MDS) studies.

Molecular Dynamics (MD) simulation studies

In order to estimate the molecular interaction stability and sustainability between the docked mucin and collagen Molecular dynamics (MD) simulations were performed using GROMACS software. MD simulation was initiated by applying the all-atom OPLS forcefield to the entire mucin-collagen complex and a cubic box with a Periodic Boundary Conditions (PBC) of 10nms.from all sides and edges of the protein complex. TIP3P water model was used for solvation of the entire system. 1000 step Energy minimisation was performed using verlet algorithm. Restraining potentials were applied to the protein and the MD simulation were carried out in the isothermal-isobaric (NPT) ensemble at 300 K and 1 atm. Temperature (v-rescale) and pressure (Berendsen) were controlled by using weak coupling thermostat. Electrostatic interactions were treated by means of Particle Mesh Ewald (PME) approach. Lennard-Jones interactions were cut-off at a distance of 10 Å, with a smooth switch-off starting at a distance of 10 Å. MDS was performed at 300 K in the canonical (NVT) ensemble. The LINCS solver algorithm was used with all bond restraints. A total production MD with a total time scale of 10ns. (10000ps.) was performed with an integration time step of 2fs. After the successful completion of MDS, the entire trajectory was analysed for the RMSD (Root Mean Square Deviation), RMSF (Root Mean Square Fluctuations) and Radius of Gyration (Rg) was calculated and the structural analysis and trajectory movie was created using Pymol. All the Simulations were performed in the High-performance computing cluster of ILS, Bhubaneshwar. After the MD run, structural trajectory analysis was done in Pymol and all the plots were plotted using Xmgrace tool of Grace Package.

Objective 3

Fabrication methodologies for mucin-based scaffolds for Bone tissue engineering (BTE)

In the scaffold fabrication, the ECM has always received considerable attention among researchers because of high biological compatibility, biological degradability and possibility of rapid remodeling in vivo. Two types of approaches are being considered for the fabrication of the polymeric scaffolds:

1) Thermoresponsive mucin gels
2) Enzymatic crosslinking approaches

2.2. Mineralization of biomaterials for bone tissue engineering

Mineralized biomaterials have been demonstrated to enhance bone regeneration compared to their non-mineralized analogs. As non-mineralized scaffolds do not perform as well as mineralized scaffolds in terms of their mechanical and surface properties, osteoconductivity and osteoinductivity, mineralization strategies are promising methods in the development of functional biomimetic bone scaffolds. In particular, the mineralization of three-dimensional (3D) scaffolds has become a promising approach for guided bone regeneration. In our study, two methodologies 1) enzymatic mineralization and 2) use of inorganic clays for mineral deposition.

Objective 4:

Biological evaluation prepared scaffold

When implanted in the body, the biomaterial undergoes many physiological processes which lead to several modifications in the biomaterial. The stability of the material is important after implantation, and the success of the graft depends on the capability of the material to remodel itself and to maintain cell colonization. Investigations into the material's capacity for cell colonization should be assessed in a pre-surgical step, before implantation. Microporosity and biocompatibility play an important role in cell behavior when cells are cultured in three-dimensional scaffolds.

Biological assays to evaluate the cell biocompatibility response of different 3D protein scaffolds were performed using MC3T3-E1 SUBCLONAL 4 cells (mouse calvaria preosteoclast, ATCC, CRL-2593) and C2C12 (ATCC® CRL-1772™ of Mus musculus, mouse muscle cells), cultured in alpha-minimal essential medium (α-MEM, HIMEDIA Cat No-AL221A) and Dulbecco's Modified Eagle's Medium (DMEM, Gibco Product Code.11574486) respectively and supplemented with 10% Fetal Bovine Serum (FBS, Gibco Invitrogen Cat No-16000044), antibiotic solution (0.25% Pen-Strep Gibco Cat No- 15140-122). For all experimental procedures, MC3T3-E1 SUBCLONAL 4 and C2C12 cells at passages 10-15 were used and incubated at 37^0 C with 5% CO_2.

Objective 5:

Development of in-vivo model

Bone defect are serious conditions in which a part of the bone is damaged or missing owing to trauma or surgery, and need to be repaired through interventional techniques such as bone grafting. There are many animal models being used to evaluate bone graft substitutes, but the main four types are calvaria defects, long bone or segmental defect, partial cortical defect and cancellous bone defect models. The development of in vivo model is being proposed to be performed.

IV. RESULTS AND DISCUSSION

Objective-1

Prior to developing any biomaterial using Mucin, The protein was detected with Coomassie Blue staining. The bands for the mucin protein, behaved anomalously, migrating as three broad bands with an apparent molecular weight of 240 kDa, 62 kDa and 55 kDa in the SDS-PAGE (lane 3). The SDS-PAGE gel of mucin with three different molecular sizes of bands was cut and processed for MALDI analysis to confirm the presence of mucin protein. The Mascot search results and Mascot score histogram along with the table validates the best protein accession along with best protein score and best protein description. The nature and extent of the secondary structure in mucin were determined by using CD spectroscopy. The CD spectrum of mucin is characterized by a large negative minimum in between 200-210 nm [4]. Analysis of the spectrum predicts that mucin contains 21.8% helical structure with 35.8 % antiparallel structure. These results indicate that a considerable portion of the mucin molecule is lacking a traditional secondary structure and that the confirmation of the native molecule is consistent with an extended non-globular structure.

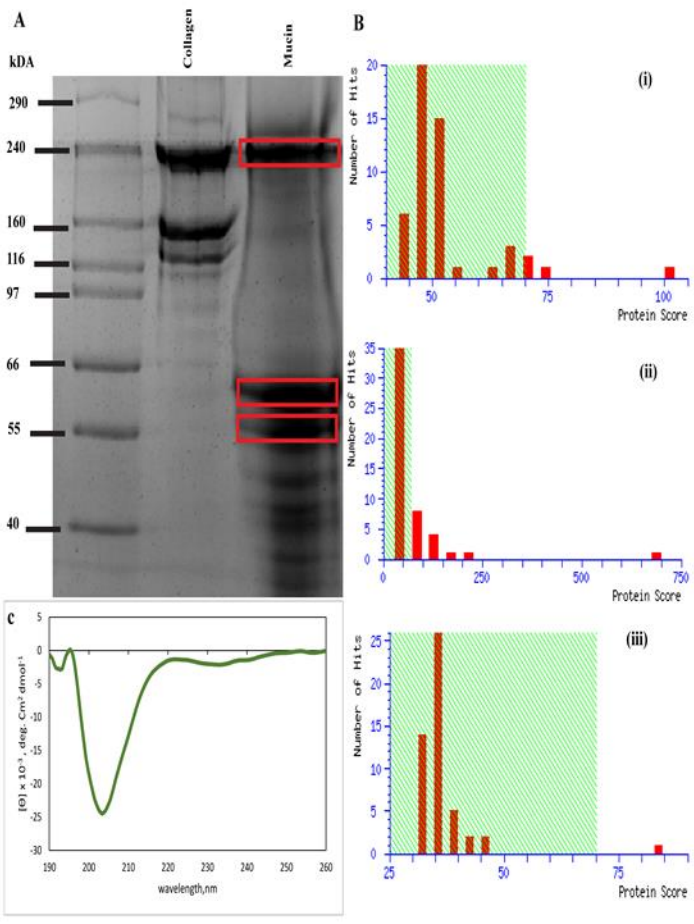

(iv)	Protein scores greater than 70 are significant (p<0.05). Database : UniProtKB-SwissProt sprot_20150527 (548586 sequences; 195452300 residues			
Molecular weight	Best Protein Accession	Best Protein Mass	Best Protein Score	Best Protein Description
55	ALBU_BOVIN	71244	101	Serum albumin OS=Bos taurus GN=ALB PE=1 SV=4
	ALBU_BOVIN	71244	81	Serum albumin OS=Bos taurus GN=ALB PE=1 SV=4
62	ALBU_BOVIN	71244	688	Serum albumin OS=Bos taurus GN=ALB PE=1 SV=4
	ALBU_BOVIN	71244	609	Serum albumin OS=Bos taurus GN=ALB PE=1 SV=4
240	VSR_BNYVS	15206	62	Probable suppressor of RNA silencing OS=Beet necrotic yellow vein virus (isolate Japan/S) GN=ORF7 PE=4 SV=1
	MUCS_BOVIN	60587	84	Submaxillary mucin-like protein OS=Bos taurus PE=2 SV=1

Figure 1. Characterization of Mucin protein. (A) SDS page gel run image showing mucin 3 bands marked within red box loaded in lane 3 along with ladder and collagen as experimental control in lanes 1 and 2 respectively. (B) MALDI TOF TOF analysis of SDS page gel image after gel digestion, Mascot score histogram of three different molecular weight i) 55 kDa, ii) 62 kDa, iii) 240 kDa, iv) Table showing all the different molecular mass 2D gel analysis matched with Uniport database. (C) Circular Dichroism Spectrum of mucin showing the far-UV at around 200 nm wavelength, maximum with random coil secondary structure.

Objective 2:

<u>In Silico-approach for pathway analysis</u>

String dB tool is being used in order to know the interaction between the bone genes along with Mucin and the interaction analysis was followed by gene ontology pathway analysis in which the m-RNA linked with Mucin gene was evaluated first then mirwalk tool was used to know relevant biological processes.

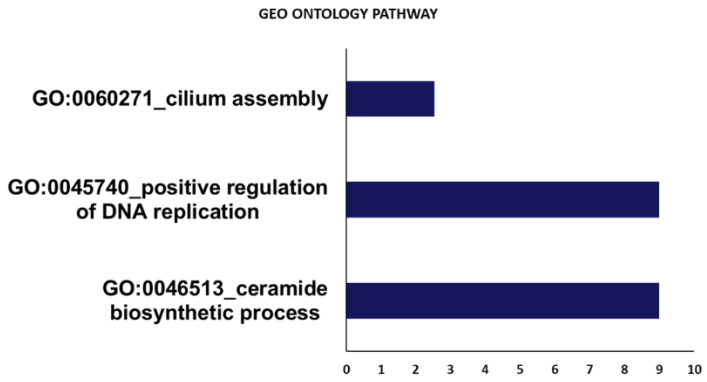

Figure-2: Bioinformatics analysis; Gene ontology analysis showing different pathway enrichment of Mucin

Modelling and molecular docking of Collagen and Mucin:

Ab-Initio structural predictions help us to know about the molecular architecture of the biomolecules, whose structure is neither experimentally determined nor they can be modelled through comparative homology modelling (whose sequence similarity should be around 30% with experimentally determined protein structures). In our case, the Collagen (Bovine) which we have used for the entire study doesn't have a great homology with experimentally determined fiber diffraction models with PDB ID: 3HQV and other crystal structures such as, 2F6A , 4AU2, 4AU3, 4AU4, 4AXY have a very small peptide structure which is co-crystallized with their respective binding partners. Similarly, Mucin protein didn't have much structural homology with experimentally determined structures. So, Mucin three-dimensional structure was predicted in an ab-initio method using the Robetta server and validated as mentioned in the methods section.

With the predicted information of Mucin and collagens binding cavities, we have proceeded for protein-protein interactions using HADDOCK. After docking the final docked conformation was chosen based on the energetics and clustering statistics. The top 4 best-docked complexes were clustered with a HADDOCK score (Binding score) of -159.2 +/- 24.6 kcal.mole-1. This cluster of 4 docked complexes has an average buried surface area of 1705.9 +/- 160.2 Å2 and a Z-Score of -1.7 Å which suggest that all these 4 structures have similar docked conformations. The Mucin was represented in yellow transparent surface and collagens triple helices were represented as green, cyan and magenta transparent surfaces. Among these 4 complexes, residue level and atomistic-level interactions analysis revealed that the collagen triple helices Proline (P) and Glycine (G) residues shown to have hydrogen-bonded contact with mucins Arginine (R), Lysine (K), Glutamate (D) and Tyrosine (Y), these H-bonded interactions between charged residues suggest to have a probable affinity between both proteins. Apart from these interactions, plenty of Van der Waal's pi-pi interactions were observed between hydrophobic residues such as Alanines (A), Prolines (P) of Collagen and Iso-leucines (I), Methionine (M) and Cysteines (C) of Mucines. These detailed interaction maps. These observed van der Waals pi-pi between semi-aromatic and aromatic residues indicate the possibility of proper hydrophobic affinity among the mucin and collagens.

Molecular Dynamic Simulations (MDS) of Collagen and Mucin Complex:

The in-silico protein-protein interactions analysis of Collagen-Mucin predicts that these proteins have a sufficient affinity towards each other. In order to check their interactions stability and sustainability, we have performed a small scale MD simulations. Prior to the MD Simulations, the collagen and mucin systems was hydrated and neutralised as described in the methods. The energy minimisation was done successfully in 827 steps, later after NVT equilibration, it was observed that the temperature during the equilibration process was maintained constantly. After the successful MD simulation run, the trajectory was analysed for RMSD (Root mean square deviation) and Root Mean Square Fluctuation (RMSF). RMSD

of collagen-mucin complex indicates the entire MD timeline the structural deviations are little from its original positions, where RMSD of the initial structure (Red) and Structural complex after equilibration (Black) suggests that a little or negligible deviation was observed. Radius of Gyration (Rg) analysis which suggests that during the MD simulation decrease in Rg indicates that both collagen and mucins terminal ends are coming closer to each other suggesting an increase in proximity with each other. Apart from this, the entire MDS trajectory was structurally visualised using pymol, where we can observe the sustainability of the interactions throughout the MD time scale.

From this molecular modelling and protein-protein docking studies of collagen-mucin suggesting to have a proper affinity towards each other. Their stability and sustainability of their interaction were further proved in 10ns. MD simulation studies. These in-silico studies paved a clear way to use collagen and mucin in-vitro for our further studies.

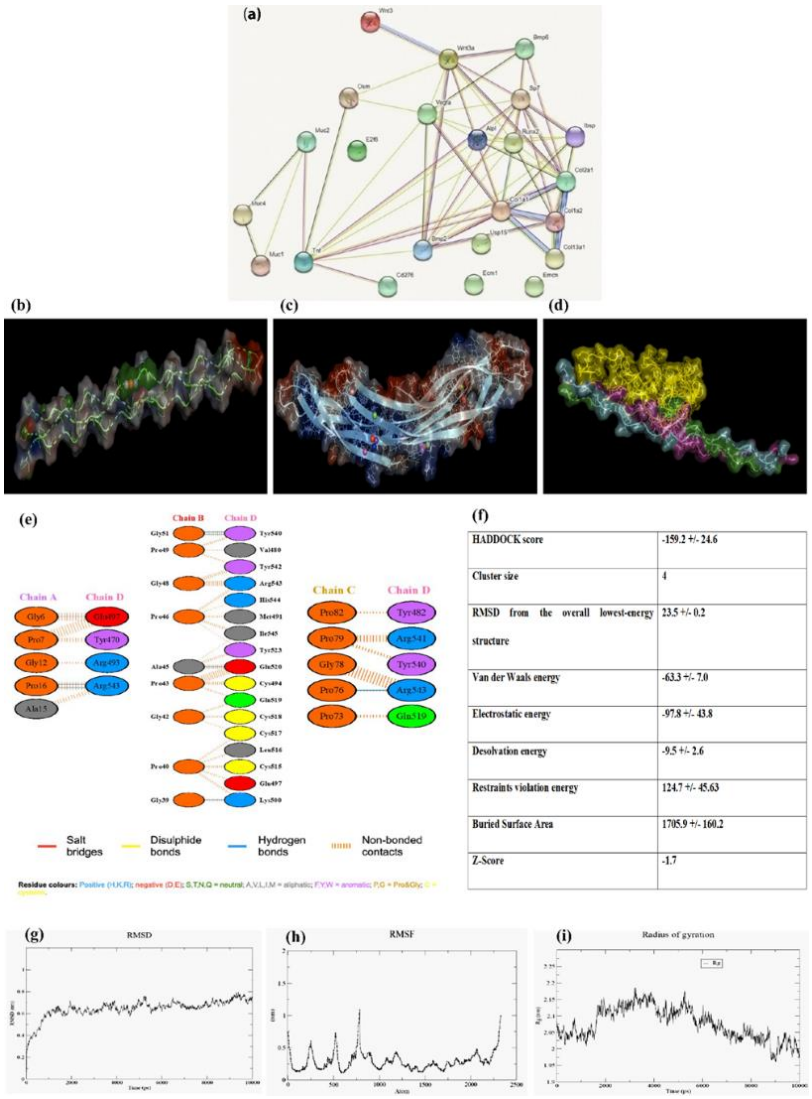

Figure 3. Bioinformatics analysis; a) Represents the interaction of Mucin gene with the genes involved in bone mineralization, Modelling and molecular docking of Collagen and Mucin. Predicted structures of Collagen and Mucin with their predicted binding sites, (b) Ab-initio predicted three-dimensional structure of collagen with its triple-helical architecture. In this the, coloured spheres indicate the predicted binding site regions, Red (PASS), Purple (Fpokcet), Green (Surfnet), Blue (Consurf), (c) Ab-initio predicted 3D structure of Mucin and its predicted binding cavities. Docked complex of Collagen Mucin and its detailed interaction maps, (d) Surface representation of Collagen-Mucin complex using HADDOCK. This complex representation is prepared using pymol. Mucin was represented with transparent yellow surface and Collagen was represented with Green, Cyan and Magenta coloured transparent surface protein, (e) the

detailed interaction map of Collagen and Mucin, where the blue lines represent the presence of H-bond and red dashed lines indicate the Van der Waals interactions. RMSD and RMSF analysis of the 10ns. MD simulation of Collagen and Mucin complex, (f) Predicted Energies and other parameters of Collagen-Mucin Docking by HADDOCK. In this HADDOCK score indicates the binding energy. All the energetic parameters are in kcal.mol-1 and buried surface area is in Å2, (g) RMSD analysis of the collagen mucin complex, in this MD after 2ns. The trajectory seems too stabilised, indicating the slight deviations in the trajectory, (h) RMSF analysis indicating the slight fluctuations observed in many residues, (i) Radius of Gyration (Rg) analysis of Collagen and Mucin: Rg analysis of the entire trajectory indicates the decrease in distance between the distal ends of both proteins suggesting a better affinity which can be observed by the overall decrease in Rg.

Objective: 3

2.1. Polymer Scaffold Preparation

A) Mucin based scaffold

The first approach of scaffold preparation included a simple interpenetrating network wherein mucin and collagen are interwoven without any covalent linking among them in a matrix consisting of crosslinked PEG network. The idea behind this approach was to use minimum chemical treatment during scaffold preparation to render the hydrogel more biocompatible. So, this approach consisted of only a single UV crosslinking step that basically crosslinked the PEG chains thereby creating the network. However, the gel fraction which is the indicator for a successful crosslinking was not promising, being less than 60%. Hence, a different approach was adopted which included the crosslinking of the two proteins collagen and mucin in the first step followed by the formation of a network structure of PEGDM in the second step. The two proteins, collagen and mucin are crosslinked using EDC-NHS by employing the carboxyl and amine groups of the two proteins. The vinyl end functionalized PEG's contain an active C=C which can be easily utilised for a UV based polymerization reaction [5]. At the end the scaffolds are prepared using two different chemistries in two steps, leading to a scaffold with better mechanical support [6].

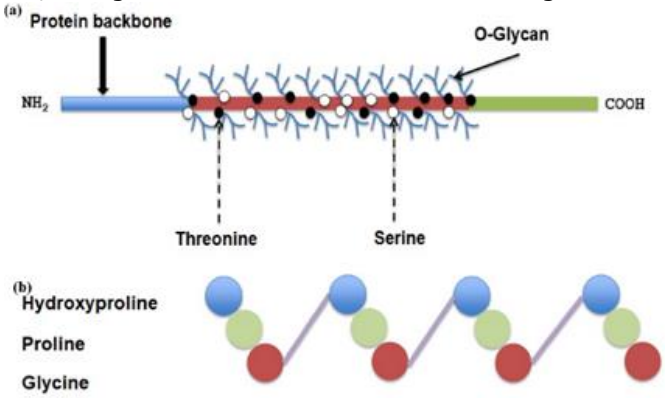

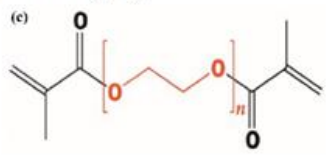

Figure 4: The chemical structures of a) Mucin. Mucin is a heavily glycosylated protein produced by epithelial tissues in animals, b) Collagen. Collagen is one of the main structural protein in the ECM of several tissues, c) PEGDMA. It is a polyether with end-capped methacrylates.

Physicochemical Characterization of the scaffolds

The porous 3D collagen-mucin based scaffolds were produced by applying a freeze-drying process. Freezing at temperature -20°C and subsequent lyophilization led to an interconnected porous system with pore diameters of 50-100μm . The different scaffolds with varying ratios of collagen and mucin didn't show remarkable difference in porosity. The blank DM5A did not have any porous structures in the morphology while the only protein scaffolds did show some porosity along with the combination scaffolds.

The complex moduli of scaffolds of different protein combinations were determined using rheology. G'signifies the storage modulus while G'' indicates the loss modulus of the scaffolds. In other words, G' is the gels ability to store deformation energy in an elastic manner. This indicates that G' can give a direct idea on the extent of crosslinking as well. An frequency angular sweep oscillatory experiment is shown in Figure 4b. Amongst the scaffolds, the presence of protein increases G' or the strength of the scaffolds as is clearly observed in the combination scaffolds (collagen+mucin+PEG) upon comparison with the blank scaffold DM5A (only PEGDMA) which does not contain any protein. Interestingly, the protein scaffolds (CDMA (collagen +PEGDMA) and MDMA (mucin+PEGDMA) with the presence of only one protein had the highest G' .

Figure 4e shows typical Raman spectrum, the presence of bands at 960 cm−1 are characteristic of the vibrational modes of phosphate. All the samples, except CDM5A and MDM5A show the characteristic peak at 960 cm−1 at 28 days post seeding where M1C2DM5A shows the maximum intensity. To our surprise, the blank DM5A also shows a peak at 960 cm−1 , which could be contamination arising from

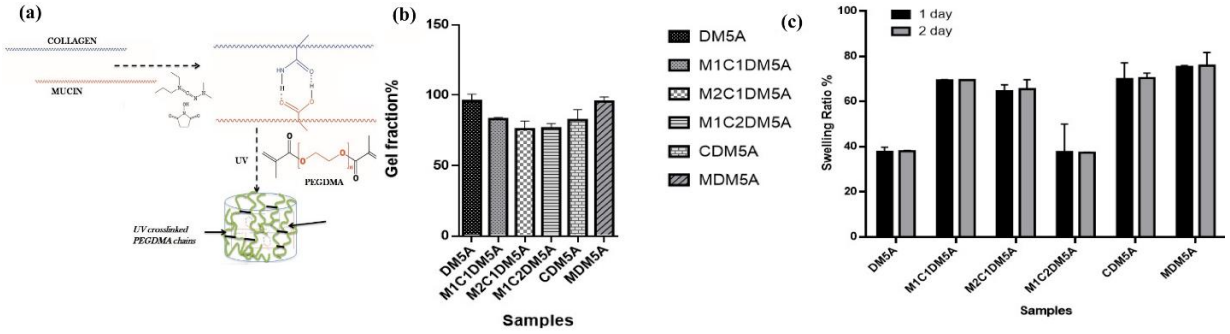

the calcium glycerol phosphate medium .

Figure 5: (a) Schematic diagram representing the two step crosslinking to prepare double networked scaffolds. (b) Gel fraction ratio% of scaffold prepared by double crosslinking technique, (c)Equilibrium swelling ratio % of scaffold prepared by double crosslinking technique.

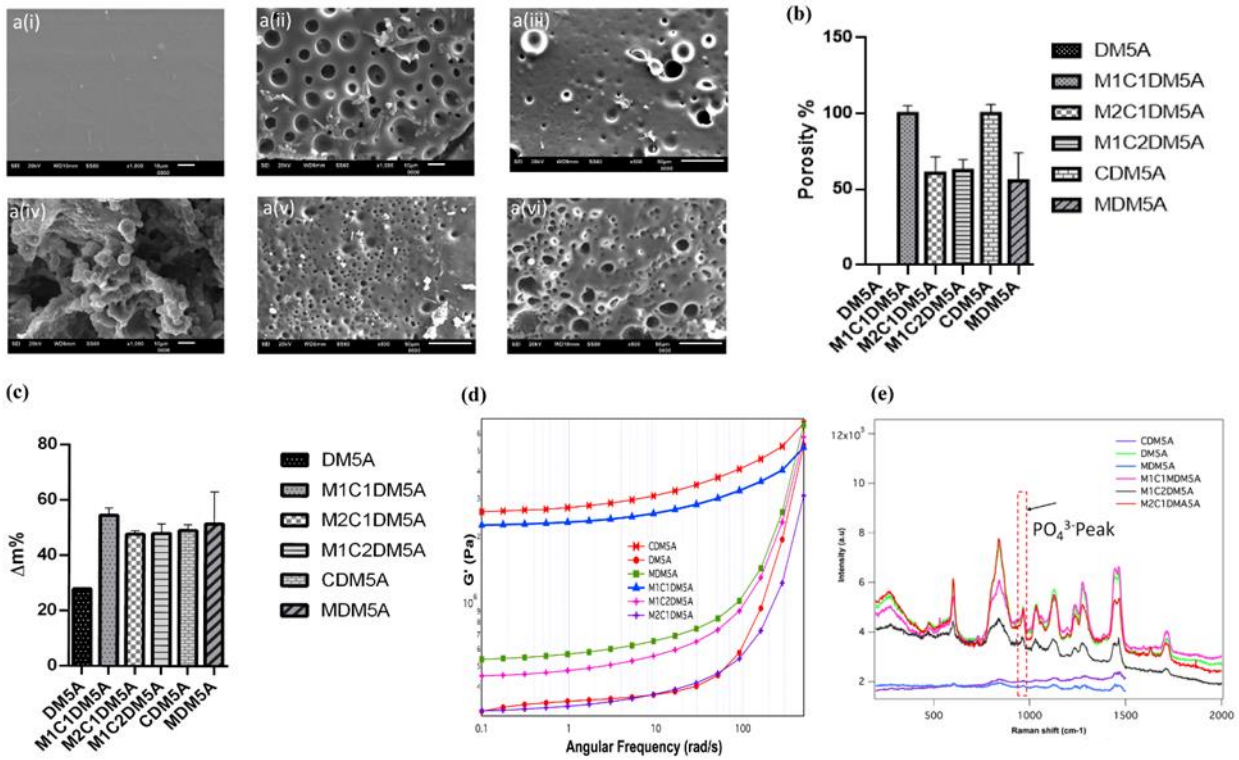

Figure 6: (a) SEM images of i) DM5A, ii) M1C1DM5A iii) M2C1DM5A iv) M1C2DM5A v) CDM5A vi) MDM5A, (b) Porosity determination using ethanol displacement technique, represented as %. (c) In-vitro biodegradation by collagenase activity (d) Rheological measurements showing the relation between G' versus angular frequency of different samples at 500 angular frequency (rad/s), (e) Raman spectra of the protein scaffolds showing the indicative peak at 960 cm-1 within the insert which confirms the presence of phosphate peak after 28 days post seeding.

A) Injectable scaffold using PNIPAM

<u>Characterization of PNIPAM conjugated mucin scaffold</u>

Conjugated PNIPAM and mucin was evaluated with sodium dodecyl sulfate-polyacrylamide gel electrophoresis (SDS-PAGE) using 8% polyacrylamide gel taking mucin in 1xPBS at the concentration of two different concentration 20mg.ml and 40mg/ml. Then we diluted the hydrogel for SDS-PAGE gel run at the concentration of 30 µg and loaded 30 µl of with high molecular weight protein ladder. Molecular mass markers were purchased from (Thermo fisher scientific, # Cat No. LC 5688) and the gel was stained with Coomassie blue R-250 using the manufacture's protocol.

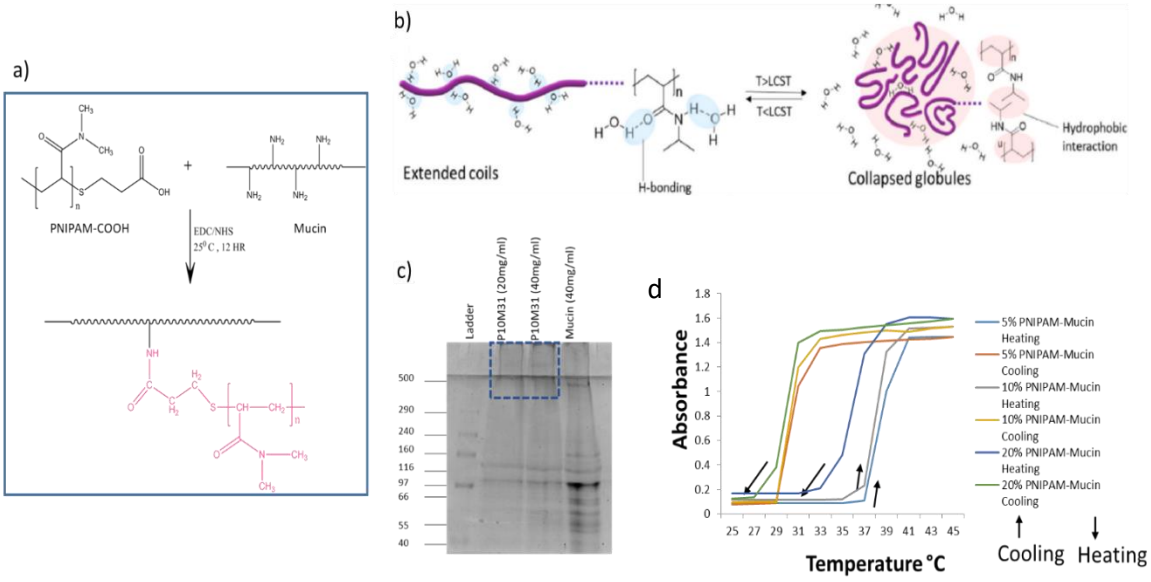

Figure 7: a) Schematic diagram of the PNIPAM conjugation after EDC-NHS ,b) Hydrophobic bond formation after hydrogel formation C. conjugated hydrogel solution at 37^0C after 2hours of incubation. c) SDS gel image with lane 1: Ladder, 2: 20mg/ml of the conjugated protein, 3: 40mg/ml of conjugated protein, 4: Mucin , blue marked region showing the smeared band because of PNIPAM conjugation,

2.2. Physicochemical characterization of the mineralized scaffolds

A) ALP treated scaffold

From the morphological analysis using scanning electron microscopy, there is a clear evidence of mineral deposition upon treatment with ALP. The deposited minerals appear as white floccules randomly distributed over and within the pores of the scaffolds. ALP mediatiated mineral deposition is known to depoit minerals with different Ca:P ratio which differ in structures ranging from plate like structures to powder like deposition . In this case the deposition was mainly observed in and around the pores. In Fig 7b we have done indirect mass increase charaterization of ALP treated scaffolds and compared it with without ALP treated scaffold (uncrosslinked) to confirm that after ALP treatment there is increase in weight which we could from the graph. The raman spectra after 28 days of scaffold treatment with ALP. The presence of PO43- is observed in all the combination scaffolds where both the proteins are present. No peak is observed in case of CDM5A and MDM5A which doesn't have both the proteins present. There was no significant change between +ALP treated and -ALP samples. The G' of the scaffolds with ALP treatment (+ALP) are higher than –ALP samples except, CDM5A and M1C1DM5A. Although there is no diret explanation for this behaviour of the two samples, but it hypothised that this corresponds to the presence of minerals. The samples which have higher deposition of minerals are brittle lacking the strength and elasticity. This explains the unusual behaviour of M2C1DM5A which has the highest deposition of minerals.

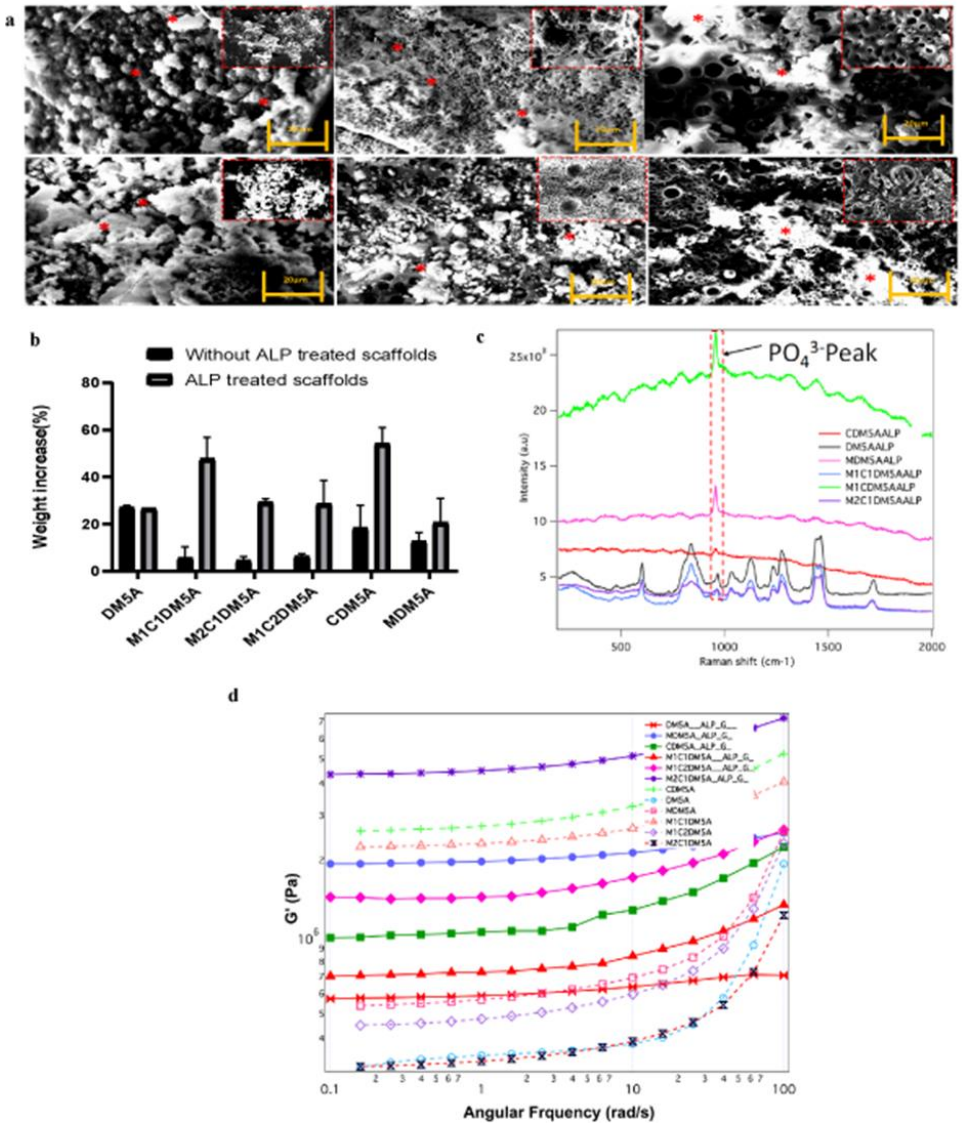

Figure 8: (a) SEM images of i) DM5A, ii) M1C1DM5A iii) M2C1DM5A iv) M1C2DM5A v) CDM5A vi) MDM5A, (b) Porosity determination using ethanol displacement technique, represented as %. (c) In-vitro biodegradation by collagenase activity (d) Rheological measurements showing the relation between G' versus angular frequency of different samples at 500 angular frequency (rad/s), (e) Raman spectra of the protein scaffolds showing the indicative peak at 960 cm-1 within the insert which confirms the presence of phosphate peak after 28 days post seeding.

B) Synthesis of (chitosan-mucin)-g-poly HEMA hydrogel scaffold

The whole reaction mechanism of the synthesis process can be separated into two distinct parts, the first is the coupling reaction assisted by carbodiimide between mucin and chitosan; the second is the free radical copolymerization reaction between chitosan and hydroxyethyl methacrylate (HEMA) monomers. EDC-NHS assisted reaction was done to form an amide bond between the carboxylic groups of mucin and the amine groups of chitosan [7]. The first step of the mechanism goes through the deprotonation of carboxylic H-atom and the formation of a bond between the C-atom of the carbodiimide group and the O-atom of the carboxylic group. The pH of the chitosan solution is maintained at around 6 to enable the availability of the primary amines. With the addition of chitosan in the system, the primary amine group of chitosan further attacks the carbonyl center and substitutes the NHS group to form a C-N bond between the mucin and chitosan molecules. For simplicity, we only consider the carboxylic groups of mucin and amine groups of chitosan in place of their whole structure to represent the schematic of the mechanism. The two hydroxyl groups in each unit of chitosan can act as a potential site for a free radical generation. Ammonium persulfate is an excellent material to initiate the formation of free radicals by cleaving the peroxy bond in it at elevated temperatures. After the initiation step when these free radicals get in contact with molecules of HEMA, immediately homolytic fission of double bond took place and one after another HEMA molecules attach to propagate the chain polymerization reaction. There are two possible ways to terminate the reaction, simply by the addition of hydrogen radical or by the addition of two similar long-chain polymers that leads to the formation of graft copolymer as the final product [8]. Although there are several other possibilities for the grafting process to take place, as in the initiation step after the formation of sulphate radical anion, it also can take up H-atom from the amine group of chitosan or even can degrade the long chitosan chain into small ones by cleaving the C-O-C linkage.

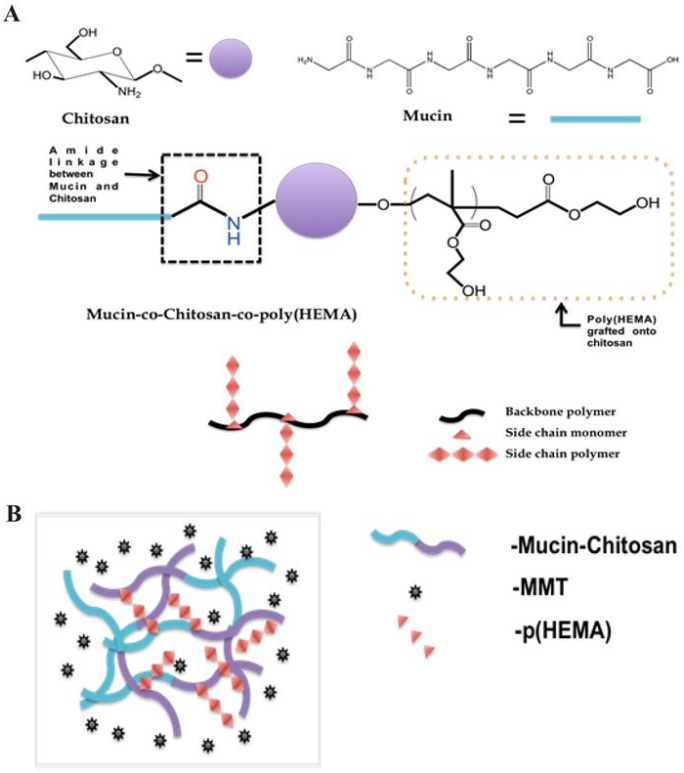

Figure 9: (A) The coupling mechanism of mucin and chitosan forming an amide bond and subsequently the grafting of the poly(HEMA) onto the chitosan backbone. (B) Representing diagram of the hydrogel formed with mucin, poly(HEMA) grafted chitosan stabilized by the presence of MMT.

Morphological and Spectroscopic analysis of the nanoclay scaffolds

SEM images of the nanoclay hydrogel obtained (Figure 4) showed a wide range of porosity in the structure. C1M2N showed some pores but surprisingly the mucin-nanoclay scaffolds did not have any pores. In general, the hydrogels did not demonstrate big pores but still exhibited reasonable water uptake capacity due to the presence of MMT. In the FTIR spectrum of chitosan we can see a broad peak from 3408-3470 cm-1 which is due to the overlapping peaks of primary, secondary O-H stretching and the symmetrical stretching of N-H bonds. The sharp peaks at 2896 cm-1 and 2857 cm-1 can be attributed to C-H stretching. The stretching of the secondary amide group present in chitosan is seen in another sharp peak at 1640 cm-1. The deformation of the O-H bond and stretching of the C-O bond of alcohols are seen in 1418 cm-1 and 1076 cm-1 respectively. A sharp peak at 1153 cm-1 corresponds to the C-O-C stretching frequency. In the case of mucin, the whole spectrum is made of numerous overlapping peaks of N-H and O-H bonds present in all the amino acid units. This is why there is almost a flat region present in between 3554 cm-1 and 2955 cm-1. The synthesized hydrogel has a broad region from 3526 cm-1 to 3290 cm-1, which is proof of the coupling reaction and mucin to be present as a part of the material, as this region can be assigned to overlapping of multiple numbers of O-H and N-H bond stretching. There is one additional sharp peak at 1714 cm-1 which arises from the stretching of C=O bonds of ester present in the synthesized material which comes from the addition of HEMA in the grafting process [9].

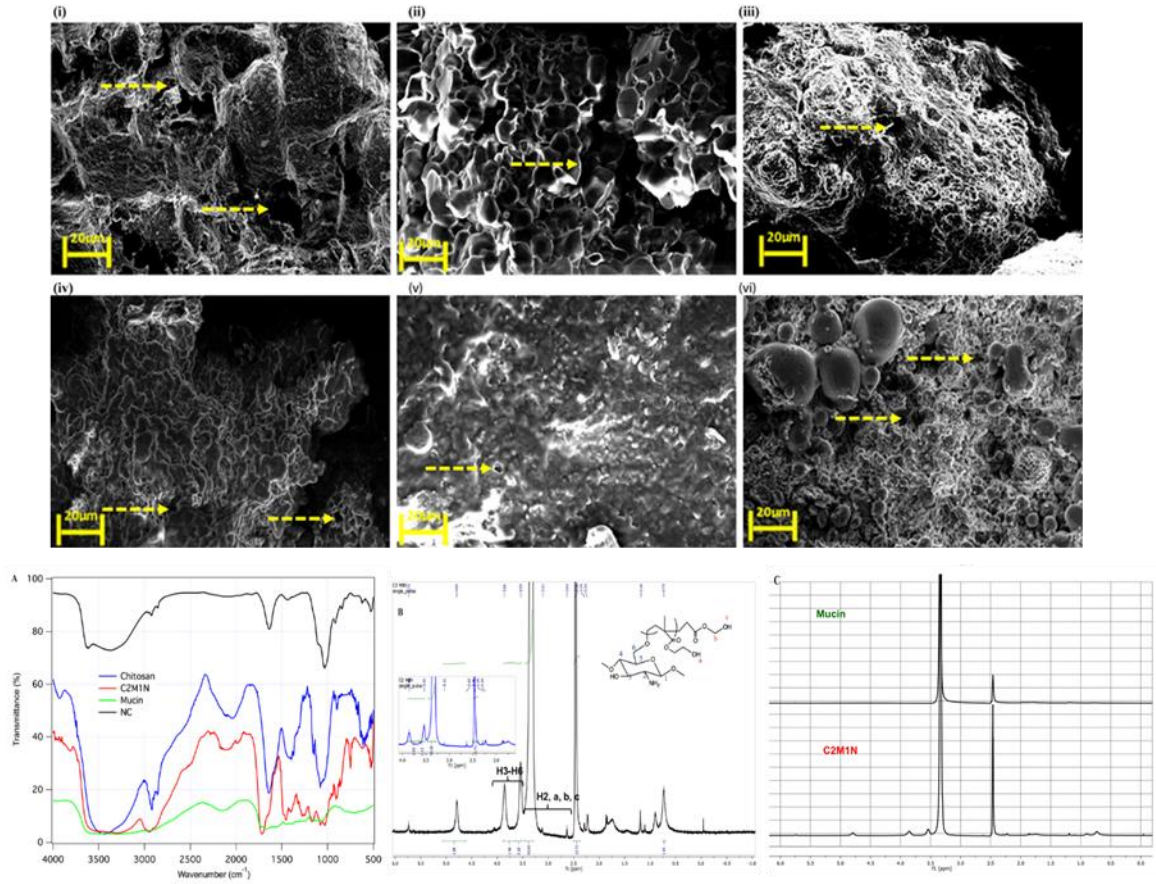

Figure 10: Scanning electron microscopy (SEM) images of top to bottom (clockwise) i) C1M1N, ii) C1M2N, iii) C2M1N, iv) NC, v) NM and vi) N. The arrows indicate the pores. FTIR image of chitosan, mucin and the composite scaffold C2M1N; NMR spectra of C2M1N showing the peak assignment, the insert indicates the zoomed area from 2.00-4.00 ppm; Comparison of the NMR spectra of Mucin and C2M1N

Objective -4

Biological evaluations of prepared scaffold

i) Mucin based scaffold

Osteogenic Differentiation of scaffolds by Alizarin assay and ALP activity

An increase in calcium content or mineralization in the protein scaffolds as was demonstrated by the alizarin red assay. M2C1DM5A scaffolds gave higher calcium content in the three consecutive weeks than either DM5A (blank) scaffold as well as the control scaffolds i.e., CDM5A and MDM5A The highest mineralization was observed for M2C1DM5A scaffolds on day 28. On the 14th and 21st day, the mineralization of all mucin-based scaffolds was significantly higher than blank scaffolds but there was no significant difference amongst the scaffolds. Moreover, the ALP activity increased at

day 21 and 28 as compared to day 14. On day 21, M1C2DM5A scaffolds showed a significant increase in ($p<0.05$) ALP activity of MC3T3-E1 cells during osteogenic induction as compared to DM5A (blank) and other scaffolds. The ALP activity was greater in the protein based scaffolds as compared to the blank at 28th day post seeding and was highest in case of M1C2DM5A

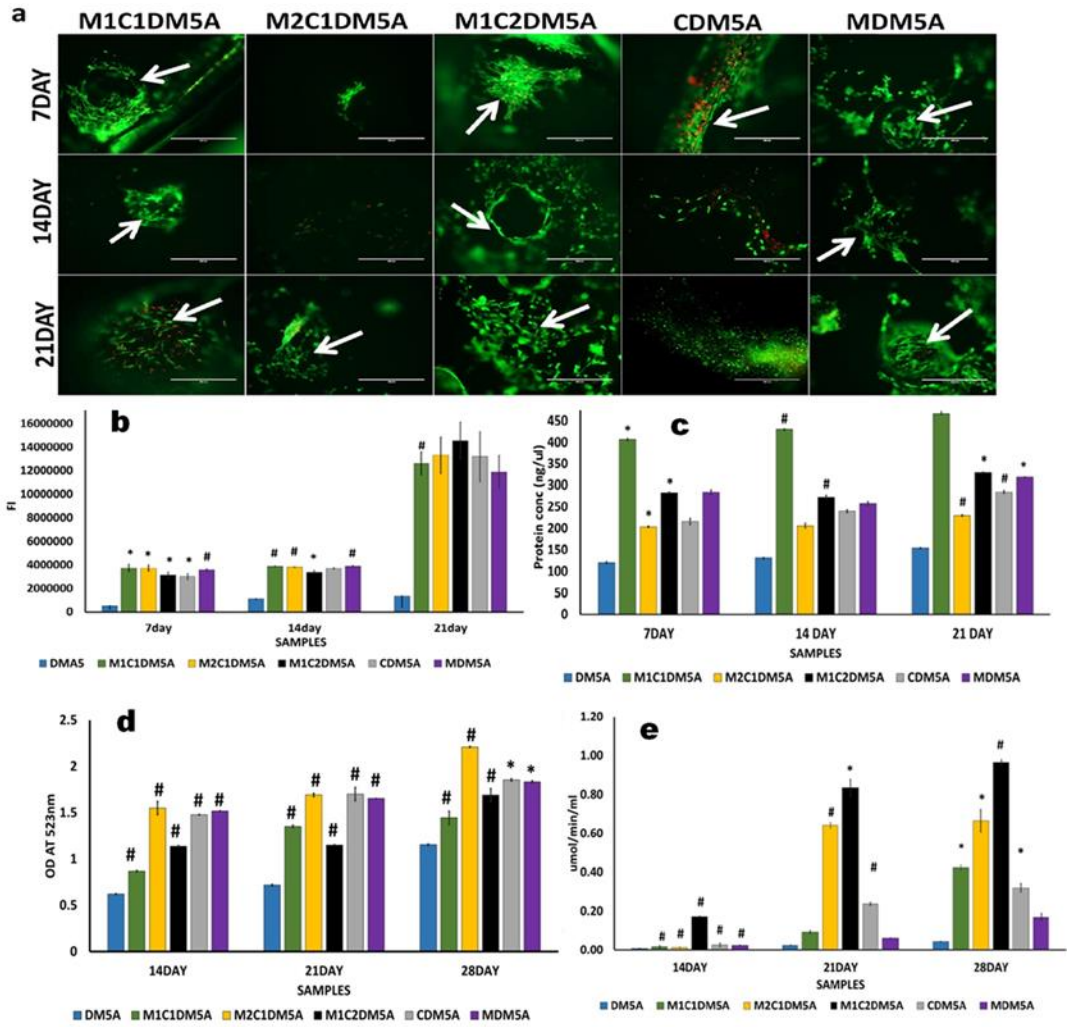

Figure 11: Cell viability and proliferation on protein based scaffolds. (a) Fluorescence microscopy (CaAM/PI staining) of MC3T3 cells cultured on the scaffolds in osteogenic medium 7, 14, 21 days post seeding; arrows indicated the adherence of cells in the pores of the scaffolds with scale bar 400um . (b) Amount of viable cells on protein based scaffolds on 7, 14, 21 day post-seeding. The amount of viable cells was quantified using the Prestoblue assay and is represented as FI (fluorescence intensity). (c)The protein content of scaffolds seeded with MC3T3 cells and cultured for 7, 14, 21 days in osteogenic

medium was determined using BCA test, (d) The amount of calcium content was calculated by the Alizarin red assay at 523 nm OD on protein based scaffolds seeded with MC3T3 cells and cultured for 14, 21, 28 days in osteogenic medium with DMA5 as blank scaffolds, (e) Alkaline phosphatase activity of cells on the scaffolds. The amount of ALP was calculated against a standard curve and normalized to total protein content. ALP activity was expressed as nanomoles (nmol) of p-nitrophenol produced per minute. MC3T3 cells were seeded and cultured for 14, 21, 28 days in osteogenic medium on protein based scaffolds. The significance was defined as #$p<0.01$, *$p<0.05$. The (#), (*) indicates significant difference compared with the control DM5A.

ii) Osteogenic studies of ALP treated scaffolds

Osteogenic Differentiation of ALP mediated scaffolds by Alizarin assay and ALP activity

The evaluation of calcium content showed an increase in calcium content or mineralization on +ALP scaffolds. +ALP treated M2C1DM5A scaffolds gave the highest calcium content in the three consecutive weeks as compared to - ALP treated and DM5A scaffold. The trend was similar in both +ALP and –ALP samples.

However, the ALP activity of +ALP treated scaffold M1C2DM5A is highest on 28th day as compared to the other samples. There was trend in increase of cell viablity of 7, 14, 21 days of postseeding in all +ALP scaffolds.

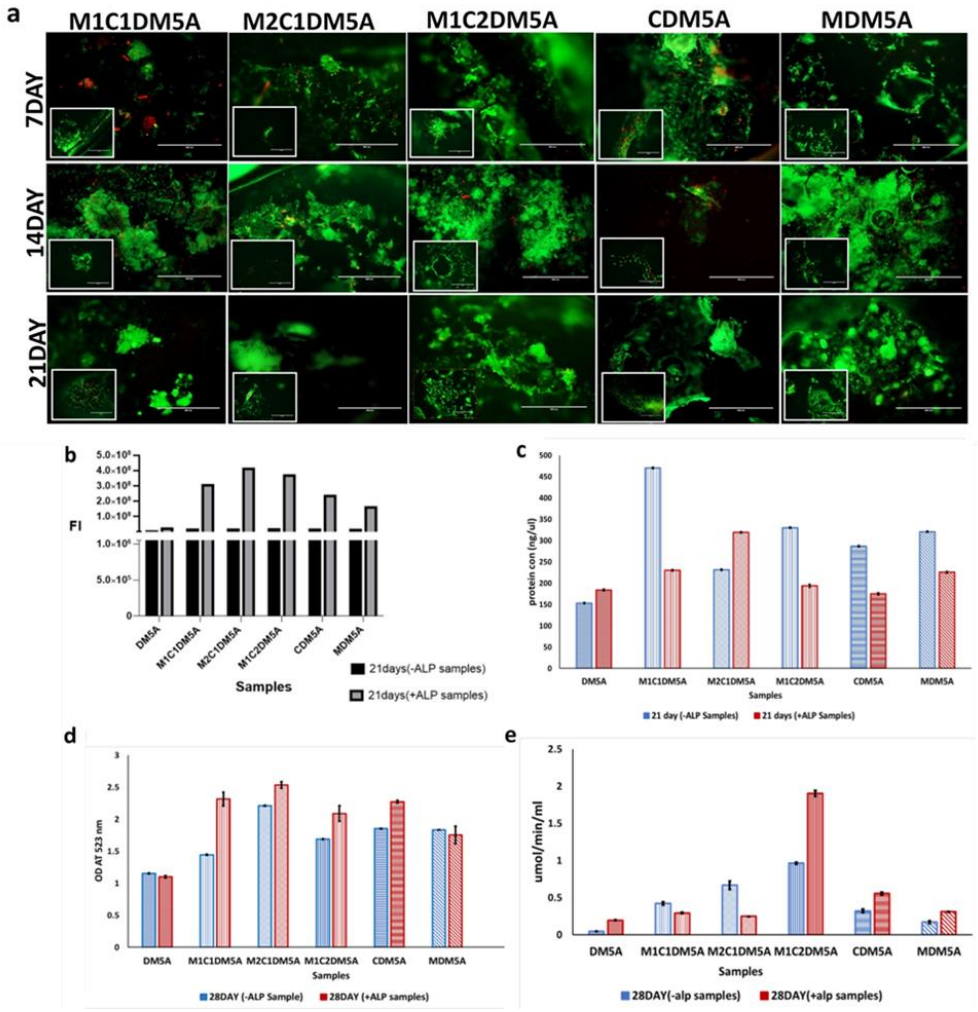

Figure 12: Cell viability and proliferation on control and protein-based scaffolds with ALP treatment. (a) Fluorescence microscopy (CaAM/PI staining) of MC3T3 cells cultured on the scaffolds in osteogenic medium at 7, 14, 21 days post seeding and the insert depicts the live and dead assay of scaffolds without ALP treatment (for comparison) with scale bar 400um, (b) Amount of viable cells on protein based scaffolds on 21 day post-seeding in comparison between scaffolds without ALP treatment. The number of viable cells was quantified using the Prestoblue assay and is represented as FI (fluorescence intensity), (c) Influence of protein based scaffold on colonization by osteogenic cells. The comparison of protein content of the scaffolds seeded with MC3T3 cells and cultured for 21 days in osteogenic medium was determined using BCA test, (d) The amount of calcium content was calculated and compared by Alizarin assay at 523 nm OD of the scaffolds seeded with MC3T3 cells and cultured for 28 days in osteogenic medium DMA5 as blank scaffolds on with and without ALP treatment, (e) Alkaline phosphatase activity on the scaffolds. The amount of ALP was calculated against a standard curve and

normalized to the total proteins. ALP activity was expressed as nanomoles (nmol) of p-nitrophenol produced per minute and compared with -ALP treated scaffolds when MC3T3 cells was seeded and cultured 28 days in osteogenic medium on protein based scaffolds with DMA5 as blank scaffolds.

C) Cell viability and proliferation on the Nanoclay scaffolds

Implantable biomaterials should be primarily non-toxic to the cells [10]. The three key requirements in tissue engineering include signals, cells that can respond to morphogens and scaffolds that are biomimetic thus mimicking the extracellular matrix. The biocompatibility of the developed hydrogels was validated with two cell lines preosteoblast, MC3T3 E1 and muscle cell line C2C12 to indicate the applicability of the developed scaffolds for wider tissue engineering applications. The rationale of choosing the cell lines also in accordance with well supported evidence from literature.

The viability of cells as determined by LIVE/DEAD® cytotoxicity assay. On day 7, the live cells layer (green fluorescence) can be observed on all composite hydrogels, which reveals that the chitosan-mucin matrix and nanoclay combination has no negative effect on the cytocompatibility. All the hydrogels promoted and indicated proliferation of cells.

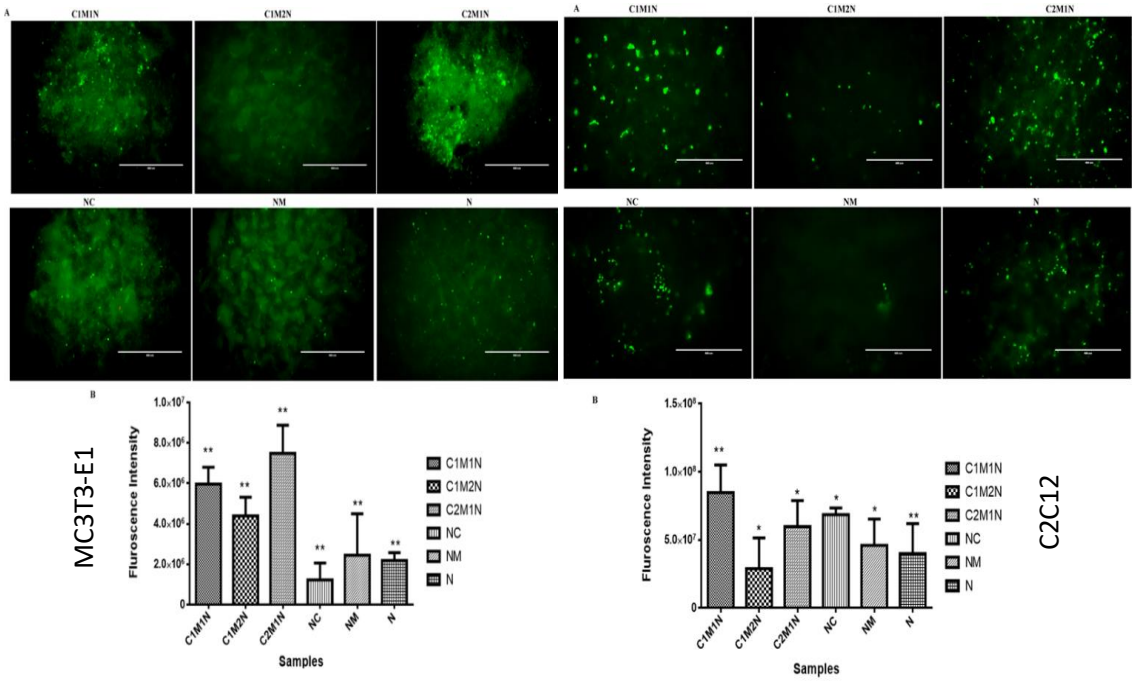

Figure 13: Two panels showing Fluorescence images of MC3T3-E1cells and C2C12 on nanoclay based hydrogel after being cultured for 7 days determined by live/dead assay on right and left panel

respectively and shows the proliferation of MC3T3-E1 and C2C12 after being cultured for 7 days on nanoclay hydrogels. *($p < 0.05$) and**($p < 0.01$) indicate statistical significance.

V. CONCLUSION

A biomimetic scaffold comprising of mucin and collagen for bone regeneration is the central focus of the research. In view of this double network, systems with PEGDMA are prepared by varying the ratio of the two proteins, mucin and collagen and to observe the effect of each protein on scaffold characteristics and cellular interaction. The successful preparation of the scaffolds is followed by in-situ deposition of mineral crystals using alkaline phosphatase mediation. The prepared scaffolds are characterized morphologically and proved to have pores that further help in crystal deposition upon ALP treatment serving as nucleation sites. In parallel, different chemistries utilizing Mucin has been employed to see the feasibility of developing hydrogels. The materials developed so far have been promising from the in-vitro studies. The next step is to develop an appropriate in-vivo model to study the regeneration ability of the polymer scaffolds. Through, this proposal it is planned to develop such in-vivo models for understanding the in-vivo applicability of the hydrogels.

VI. IMPACT OF THE RESEARCH IN THE ADVANCEMENT OF KNOWLEDGE OR BENEFIT TO MANKIND

In last decade, tissue engineering has moved a way ahead and has proposed solutions by replacing the permanently or severely damaged tissues of our body. The field has expanded to tissue regeneration of cartilage, bone, blood vessels, skin, etc. The domain of tissue engineering is very wide and is the combination of bioengineering, biology & biochemistry.

Bone tissue engineering has emerged as one of the leading fields in tissue engineering and regenerative medicine. The success of bone tissue engineering relies on understanding the interplay between progenitor cells, regulatory signals, and the biomaterials/scaffolds used to deliver them – otherwise known as the tissue engineering triad. Moreover, different materials can exert different biomechanical forces, several factors such as material architecture can profoundly affect cellular differentiation and migration in a cell type specific manner. Understanding these interactions will be critical for enhancing the progress of bone tissue engineering towards clinical applications. The current project focuses on an improvement of our understanding of chemical and biological processes involved in the preparation characterization of extra cellular matrix-based protein system as resorbable bone graft substitute and their evaluation in the bone formation and mineralization.

The outcome of the project will lead to the use of safe and inexpensive biomaterial as bone graft for critical sized defects. This project will provide substantial information and knowledge in translation research of biomedical sciences in order to further enhance the applicant's potential for a successful career in biomedical research.

VII. LITERATURE REFERENCES

[1] Z. Paknejad, M. Jafari, P. Nazeman, M. Rezai Rad, A. Khojasteh, 24 - Periodontal and peri-implant hard tissue regeneration, in: L. Tayebi, K. Moharamzadeh (Eds.), Biomaterials for Oral and Dental Tissue Engineering, Woodhead Publishing2017, pp. 405-428.

[2] F. Han, J. Wang, L. Ding, Y. Hu, W. Li, Z. Yuan, Q. Guo, C. Zhu, L. Yu, H. Wang, Z. Zhao, L. Jia, J. Li, Y. Yu, W. Zhang, G. Chu, S. Chen, B. Li, Tissue Engineering and Regenerative Medicine: Achievements, Future, and Sustainability in Asia, 8(83) (2020).

[3] G. Petrou, T. Crouzier, Mucins as multifunctional building blocks of biomaterials, Biomaterials science 6(9) (2018) 2282-2297.

[4] N.J. Greenfield, Using circular dichroism spectra to estimate protein secondary structure, Nat Protoc 1(6) (2006) 2876-2890.

[5] A. Bagheri, J. Jin, Photopolymerization in 3D Printing, ACS Applied Polymer Materials 1(4) (2019) 593-611.

[6] A. Haider, S. Haider, M. Rao Kummara, T. Kamal, A.-A.A. Alghyamah, F. Jan Iftikhar, B. Bano, N. Khan, M. Amjid Afridi, S. Soo Han, A. Alrahlah, R. Khan, Advances in the scaffolds fabrication techniques using biocompatible polymers and their biomedical application: A technical and statistical review, Journal of Saudi Chemical Society 24(2) (2020) 186-215.

[7] J. Bart, R. Tiggelaar, M. Yang, S. Schlautmann, H. Zuilhof, H. Gardeniers, Room-temperature intermediate layer bonding for microfluidic devices, Lab on a Chip 9(24) (2009) 3481-3488.

[8] M. Semsarilar, V. Abetz, Polymerizations by RAFT: Developments of the Technique and Its Application in the Synthesis of Tailored (Co)polymers, Macromolecular Chemistry and Physics 222(1) (2021) 2000311.

[9] M. Nikdel, M. Salami-Kalajahi, M. Salami Hosseini, Synthesis of poly(2-hydroxyethyl methacrylate-co-acrylic acid)-grafted graphene oxide nanosheets via reversible addition–fragmentation chain transfer polymerization, RSC Advances 4(32) (2014) 16743-16750.

[10] M. Saini, Y. Singh, P. Arora, V. Arora, K. Jain, Implant biomaterials: A comprehensive review, World J Clin Cases 3(1) (2015) 52-57.

Debyashreeta Barik

Applicant

Debyashreeta Barik

3rd Year Ph.D. student,

Institute of Life Sciences,

Bhubaneswar